MINISTRY OF SUPPLY

AERONAUTICAL RESEARCH COUNCIL
REPORTS AND MEMORANDA

Pressure Plotting Tests in the Royal Aircraft Establishment High Speed Wind Tunnel on a 21 per cent Thick, Low Drag Aerofoil (Brabazon I Wing Root Section)

By

A. B. HAINES, B.Sc. and W. PORT
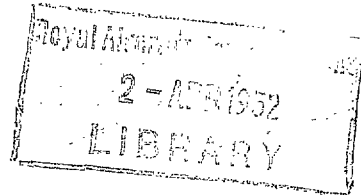
LONDON : HER MAJESTY'S STATIONERY OFFICE

1952

PRICE 6s. 6d. NET

Pressure Plotting Tests in the Royal Aircraft Establishment High Speed Wind Tunnel on a 21 per cent Thick, Low Drag Aerofoil (Brabazon I Wing Root Section)

By

A. B. Haines, B.Sc. and W. Port

Communicated by the Principal Director of Scientific Research (Air), Ministry of Supply

---

Reports and Memoranda No. 2617*

October, 1947

Summary.—Pressure plotting tests have been made on the 21 per cent thick wing root section for the Brabazon I aircraft as a two-dimensional aerofoil spanning the Royal Aircraft Establishment High Speed Tunnel. The tests covered a Mach number range up to 0·7 at a Reynolds number of about 3×10^6 and low speed tests were extended up to $R = 9·45 \times 10^6$.

The results have shown that:—

(i) No serious compressibility effects on C_L and C_m occur in the cruising conditions (M up to 0·6, C_L up to 0·66).

(ii) $C_{L\ max.}$ remains roughly constant at about 1·15 up to $M = 0·6$, and then falls to 1·01 for $M = 0·7$.

(iii) For $M = 0·2$, $C_{L\ max.}$ increases from 1·17 for $R = 3 \times 10^6$ to 1·26 for $R = 9·45 \times 10^6$.

(iv) The reason for the maintenance of $C_{L\ max.}$ seems to be a backward movement of the peak suction which is not found on other sections.

(v) Two distinct C_L *vs.* α curves beyond the stall are obtained at low Mach number.

It appears that there is adequate margin between the cruising and stalling conditions to provide manoeuvrability and safety in up-gusts.

The results on $C_{L\ max.}$ may be pessimistic because the tunnel tests had to be made by covering the speed range at a series of certain fixed incidences (*see* section 7). Also the incidence range covered was not large enough.

Introduction.—The present report describes pressure plotting tests on a 21 per cent thick 'low-drag' section, constant chord aerofoil in the R.A.E. High Speed Tunnel. This is the root section of the wing of the Brabazon I, Mk. II aircraft, which is estimated to cruise at Mach numbers between 0·52 and 0·6 and when fully loaded, at $C_L = 0·66$. Earlier tests[1] on a conventional 21 per cent thick aerofoil (NACA 23021) showed a serious loss in lift, particularly at high incidence, for Mach numbers above about 0·5. Although it can be forecast (*see* Ref. 2) that in general, $C_{L\ max.}$ at high Mach numbers will be increased by moving the maximum thickness and camber aft along the chord following the design of 'low-drag' sections, no experimental data existed on such sections as thick as 21 per cent. It was feared, therefore, first that the

---

(21066)   A

difference between the cruising C_L, quoted above, and the $C_{L\,max.}$ at the appropriate Mach number would not be sufficient to provide adequate manoeuvrability and also that the possible increase in incidence above the cruising value before reaching the stall would not give sufficient margin to allow for up gusts.

For low Mach numbers, the actual values of $C_{L\,max.}$ and also the possible existence of kinks or subsidiary maxima in the C_L vs. α curves of ' low drag ' sections are known to be influenced by scale effect at Reynolds numbers of the order of 10^6 (see Ref. 3). At Mach numbers beyond that at which the lift begins to fall, the effects may be expected to decrease since the flow behind the shock wave will be turbulent at all Reynolds numbers. In the present tests, the two-dimensional wing was of 3-ft chord, thus enabling a Reynolds number of 3×10^6 to be achieved even at Mach numbers up to 0·7. Also, the low Mach number tests were extended up to $R = 9·45 \times 10^6$. It was hoped that with the help of such flight versus tunnel comparisons as are given, for example, in Ref. 4, these values of Reynolds numbers would be high enough to produce results that would not be misleading because of scale effect.

It is likely that similar thick, ' low-drag ' sections may be used frequently and so the results of the present tests will be applicable not only to the Brabazon I but also more generally. They provide information on how $C_{L\,max.}$, the angle for zero lift, $dC_L/d\alpha$, C_m and the form drag of such sections vary with increasing Mach number up to 0·7.

2. *Description of Tests.*—2.1. *Model.*—The wooden model of 3-ft chord and 7-ft span was mounted vertically in the R.A.E. High Speed Tunnel. No facilities were available for changing the incidence with the wind on. The aerofoil section, which was the root section of the wing of the Brabazon I, Mk. II aircraft, was designed to have a ' roof-top ' pressure distribution. A detailed table of ordinates is given in Table 1, and a sketch in Fig. 1. Its principal features are:—

maximum $t/c = 21$ per cent at $0·36c$ from the leading edge,

maximum camber $= 3·35$ per cent at $0·40c$ from the leading edge,

leading edge radius $= 0·027c$.

Compared with the NACA 23021 section, the principal difference is in the position of maximum camber, which is about $0·25c$ further aft on the Brabazon I section.

Fig. 1 also shows the positions of the 29 pressure holes; the key and the exact positions are set out in Table 2. Their average spanwise location corresponded to the tunnel centre-line (all the holes were within $\pm$ 1 in. of this line) and the pressures were led away down copper tubes in the wing to multi-tube manometers of which both visual and photographic records were taken.

2.2. *Range of Tests.*—The pressure distributions were measured at a Reynolds number of 3×10^6 over a range of Mach number up to 0·7 with the aerofoil set at seven different incidences from 0 deg to 14 deg. Tests were also made at a Mach number of about 0·2 for three values of R: approximately 2·9, 6·1 and 9·45 $\times 10^6$ for incidences (nominal) of 6, 10, 12 and 14 deg.

2.3. *Reduction of Results.*—The pressure distributions were integrated both normal and parallel to the chord and then resolved into the lift and form drag force components. At the high incidence end of the range, the force parallel to the chord represents an appreciable fraction of the lift at all Mach numbers. The pressures were also integrated to give the pitching moments which were related to the aerofoil quarter-chord point.

2

The following corrections for tunnel blockage were applied to M and $\frac{1}{2}\rho V^2$, and appropriate corrections to C_p:—

M (uncorrected)	0·3	0·4	0·5	0·6	0·65
$\varDelta M$	0·003	0·005	0·008	0·014	0·020
$\varDelta\frac{1}{2}\rho V^2/\frac{1}{2}\rho V^2$	0·021	0·0245	0·028	0·036	0·045

The contributions to the blockage due to the images of the wake were based on the measured, integrated values of form drag and a calculated estimate of the skin friction drag (which was small in comparison to the form drag).

The usual tunnel constraint corrections were applied to the lift and pitching-moment coefficients: at maximum C_L and high Mach number, these corrections amounted to about 5 per cent of the uncorrected values.

3. *Presentation of Results.*—3.1. *Effect of Mach Number* (for $R = 3 \times 10^6$).—The pressure distributions are plotted on a C_p vs. x/c basis for corrected Mach numbers of approximately 0·3, 0·5, 0·6, 0·65 and 0·7 and for the following typical incidences: 0, 4, 5·96, 7·93, 9·75 and 13·6 deg in Figs. 2 a, b, c, d, 3, 4 a, b. Fig. 5 shows the variation of $(-C_p)_{max.}$ for the upper surface with Mach number at various incidences; lines have also been drawn corresponding to local Mach numbers of 1·0, 1·3 and 1·4.

A lift carpet is presented in Fig. 6 while the values of $C_{L\,max.}$ and $dC_L/d\alpha$ for $C_L = 0·6$ are plotted against Mach number in Figs. 7a and b. It should be noted that for some of the Mach numbers (*see* Fig. 6), higher values of C_L than those shown in Fig. 7 are ultimately attained but in practice, the important C_L values are the lowest for which $dC_L/d\alpha = 0$ (*see* also section 6). Polar curves are given in Fig. 10 of C_D (form drag) against C_L for Mach numbers of 0·3, 0·5, 0·6 and 0·7 while C_m ($c/4$) is plotted against M for $C_L = 0·7$ and 1·0 in Fig. 11.

These results are discussed in section 4, while in section 6, some remarks are made concerning their application to practical conditions.

3.2. *Effect of Reynolds Number* (at low Mach Number).—The pressure distributions at a Mach number of about 0·2 are given for $R = 2·9, 6·18$ and $9·45 \times 10^6$ and $\alpha = 9·75$ deg in Fig. 12 and for the upper surface only for $R = 2·92, 6·44$ and $9·45 \times 10^6$ and $\alpha = 13·6$ deg in Fig. 13. The variation of $C_{L\,max.}$ with Reynolds number is given in Fig. 14.

4. *Discussion of Mach Number Effects.*—4.1. *Lift Characteristics.*—The following are the chief lift characteristics:—

(i) by extrapolation of the lift carpet (Fig. 6), it is clear that the no-lift angle remains constant at about -3 deg (roughly the expected low speed value) up to $M = 0·6$, beyond which it increases, reaching 0 deg for a Mach number slightly above 0·7.

(ii) At moderate incidences (*e.g.*, $\alpha = 4$ deg), Figs. 6, 7b show that C_L at constant α increases roughly as $(1 - M^2)^{-1/2}$ up to about $M = 0·5$. This increase contradicts the usual belief that for sections greater than about 17 per cent thick, there is no Glauert rise in C_L. The subsequent fall in $(\partial C_L/\partial\alpha)_M$ for $C_L = 0·6$ is shown in Fig. 7b.

(iii) From Figs. 6, 7a, it can be seen that $C_{L\,max.}$ remains constant with Mach number up to $M = 0·5$—an average value for $C_{L\,max.}$ in this range is 1·15. Between $M = 0·5$ and 0·6, $C_{L\,max.}$ increases up to 1·2 but at higher Mach numbers, $C_{L\,max.}$ decreases, being 1·01 for $M = 0·7$. As explained in section 3.1, $C_{L\,max.}$ is taken to be the lowest value of C_L for which $(\partial C_L/\partial\alpha)_M = 0$. For higher incidences, at $M = 0·2$, two distinct C_L curves can be obtained (section 5 and Fig. 15); at $M = 0·3$, C_L first falls slightly and then rises again; with increasing M up to 0·5, these variations tend to disappear. For $M = 0·6$, however, there is a fairly gentle inflexion in the

3

curve at about $C_L = 0.95$ above which C_L rises steeply to its high maximum value of 1.2. It will be shown in sections 4.2, and 5 that these changes in behaviour correspond to the fluctuations between two distinct pressure distribution shapes found for low Mach number and illustrated in Fig. 16. The significance of the results is discussed in section 7.

Remembering that it is estimated that the highest cruising speed for the Brabazon I will be $M = 0.6$, and that the cruising C_L will vary from 0.42 to 0.66 according to the load, it follows that the value of $(C_{L\,max.} - \text{cruising } C_L)$ is sufficient for adequate manoeuvrability—*see* also section 7. Also considering $M = 0.6$ (Fig. 6), the cruising incidence is seen to be about 3 deg and so there is about a 10 deg margin between the stalling and cruising incidences which should be sufficient to prevent stalling in up-gusts.

The lift characteristics bear out the general conclusion of Ref. 2 concerning the difference in the characteristics of low-drag and conventional sections. The results[1] for the NACA 23021 section showed a marked drop in $C_{L\,max.}$ with increasing Mach number, particularly at Reynolds numbers above 10^6 (*see* Fig. 1 of Ref. 2). The loss in $(\partial C_L/\partial \alpha)_M$ with M for the NACA section compared with the Brabazon I section is shown by Fig. 8 which is a comparison in the form of C_L *vs.* incidence from zero lift. Since the maximum thickness has only moved aft from 0.3 to $0.36c$, it appears that the principal cause of the very different performance of the two sections must be the position of maximum camber ($0.15c$ for the NACA 23021, $0.4c$ for Brabazon I).

4.2. *Pressure Distributions.*—The above lift characteristics can be understood more easily by reference to the pressure distributions (Figs. 2 to 5).

The low speed pressure distribution of this section at moderate incidences particularly near that giving the design C_L of about 0.45 is designed to be of the 'roof-top' variety, *i.e.*, there is a flat peak suction extending well along the chord (*see* Fig. 2b, c). For $M = 0.4$ and $C_L =$ about 0.7, this section at $\alpha = 4$ deg, has a peak suction given by $C_p = -1.55$ which remains roughly constant from $0.2c$ back to $0.4c$ from the leading edge (Fig. 2b). The NACA 23021 section, by comparison, has a sharp peak suction of $C_p = -2.18^*$ at $0.06c$ for the same lift (corresponding to $\alpha = 7$ deg). On the latter aerofoil, there is a very marked adverse pressure gradient behind the position of peak suction and in this region, increasing Mach number has little effect until shock waves have appeared. The suctions, therefore, increase with Mach number only over the extreme forward part of the aerofoil and so the change in C_L at constant incidence is small. On the present Brabazon I section, on the other hand, the peak suction being 30 per cent lower and further back, $(- C_p)$ increases both fore and aft of this position, thus leading to the observed increase in C_L (Fig. 6). Fig. 5 shows that for these moderate incidences, the limiting local Mach number is slightly less than 1.3.

Similarly, the variations in the pressure distribution shapes account for the $C_{L\,max.}$ performance. The pressure distributions shown in Fig. 3 for $\alpha = 9.75$ are typical of conditions near the stall (*see* the $\alpha = 10$ deg line in Fig. 6). As M increases up to 0.6, the peak suction moves aft from about $0.04c$ to about $0.25c$ and also the actual value of the peak $(- C_p)$ increases. These two effects help to compensate for the drop in suction over the front $0.15c$.

The effects of increasing the incidence above 9.75 deg at low Mach number is discussed in detail in section 5. As explained above, with increasing Mach number, the changes tend to disappear until $M = 0.6$ is reached. For this Mach number, $\alpha = 9.75$ deg is about at the inflexion in the C_L *vs.* α curve (Fig. 6) and the lift then shows an unexpected increase with incidence. If the changes in the pressure distributions for $M = 0.5$, 0.6 are considered, it is seen from Figs. 3, 4a that:—

    (a) for $M = 0.5$, increasing the incidence from 9.75 to 13.6 deg results in:—

        (i) a forward movement of the peak suction from $0.15c$ to $0.05c$, giving an increase in the lift contribution from the front $0.1c$, and

---

* for $R = 2 \times 10^6$; Brabazon results are for $R = 3 \times 10^6$.

(ii) a steepening and forward movement of the subsequent adverse pressure gradient, producing an earlier separation (roughly at $0 \cdot 65c$ for $9 \cdot 75$ deg and $0 \cdot 5c$ for $13 \cdot 6$ deg). The lift contribution from the portion of the aerofoil between $0 \cdot 25c$ and $0 \cdot 5c$ is seriously reduced (from $0 \cdot 36$ to $0 \cdot 25$).

These two effects roughly neutralize each other (*see* Fig. 6).

(b) For $M = 0 \cdot 6$, on the other hand, the suctions near the leading edge increase with incidence as before, but the position of maximum suction is determined by the shock wave position which, rather surprisingly, appears to remain the same from $9 \cdot 75$ deg to $13 \cdot 6$ deg (Figs. 3, 4a). Consequently, the lift contribution from the region $0 \cdot 25c$ to $0 \cdot 5c$ actually increases by $0 \cdot 03$ (*cf.* effect above for $M = 0 \cdot 5$). Further, the region of separated flow, which has certainly not spread forward, is not so well defined as the pressure near the trailing edge is still rising rather than remaining constant. The net effect of these changes is to produce the high value of $C_{L \text{ max.}}$ for $M = 0 \cdot 6$ noted in Fig. 7a.

The difference in the behaviour for $M = 0 \cdot 5, 0 \cdot 6$ are presumably due to the effect of a supersonic region on the boundary layer. Behind a shock wave the flow will probably be turbulent and it is possible that the change in the flow pattern for incidences beyond the inflexion point at $M = 0 \cdot 6$, is due to a transition from laminar to turbulent flow in the supersonic region (*cf.* discussion in sections 5 to 7).

With further increase in M beyond $0 \cdot 6$, Figs. 3, 4a show that the peak suctions, and the suctions over the forward part of the aerofoil decrease. Fig. 5 shows that the decrease in the peak suctions corresponds to a constant local Mach number. This limiting value is shown by Fig. 5 to be about $1 \cdot 35$—a result which is in agreement with the conclusions of Ref. 1 based on the tests of the NACA 23021 section. The adverse pressure gradient consequently becomes less steep but at the high incidences (Fig. 4a), the measured values of $(- C_p)$ over the rear half of the section remain constant back to the trailing edge. A result of this characteristic is that the loss in $C_{L \text{ max.}}$ between $M = 0 \cdot 6$ and $0 \cdot 7$ is somewhat retarded by the increased contribution from the rear half.

The effects of the changes in the pressure distributions on the production of lift that have just been described are best summarized by reference to Fig. 9. This shows the variation along the chord of $\Delta C_p = (C_p)_{\text{Upper Surface}} - (C_p)_{\text{Lower Surface}}$ for three different conditions :—

$$M = 0 \cdot 2, \ \alpha = 9 \cdot 75 \text{ deg}, \ C_L = 1 \cdot 18$$

$$M = 0 \cdot 6, \ \alpha = 11 \cdot 70 \text{ deg}, \ C_L = 1 \cdot 19$$

$$M = 0 \cdot 7, \ \alpha = 13 \cdot 60 \text{ deg}, \ C_L = 0 \cdot 99$$

The curves, therefore, show the distribution of force perpendicular to the chord for three conditions for which the aerofoil is about to stall (Fig. 6). It should be particularly noted that it is only for Mach numbers above $0 \cdot 6$ (*i.e.* after $C_{L \text{ max.}}$ begins to decrease with M) that the build-up of suction over the rear half of the aerofoil, where the flow has separated on the upper surface, has any appreciable effect on the value of the overall lift.*

4.3. *Profile Drag.*—The integrated values of form drag are shown for four Mach numbers— $0 \cdot 3$, $0 \cdot 5$, $0 \cdot 6$, and $0 \cdot 7$ in Fig. 10. Including an estimate of $0 \cdot 004$ for the skin friction drag, it appears that C_D for $C_L = 0 \cdot 4$ and $M = 0 \cdot 3$ would be about $0 \cdot 008$ which agrees well with

---

* If a comparison is made of the pressure distribution shapes for any Mach number for the Brabazon I and NACA 23021 sections set at incidences giving roughly the same lift, it will however be noted that much more of the lift is produced over the rear half of the section for the Brabazon I. This results from the different camber lines for the two sections—the Brabazon I section has its maximum camber at $0 \cdot 4c$ and a positive camber throughout, while the NACA 23021 section has its maximum camber at $0 \cdot 15c$ and aft of about $0 \cdot 8c$ a negative camber to give a small C_{m0}.

expectation. The form drag increases slightly with Mach number up to $M = 0\cdot5$, but by $M = 0\cdot6$, it is beginning to rise rapidly and is very large for $M = 0\cdot7$. The increases are principally due to the increasing suctions near the trailing edge, illustrated in Figs. 3, 4a and 9.

It should be noted that (except for $\alpha = 0$ deg), the values of the form drag are obtained by two successive processes, each of which involve finding the relatively small difference of two large quantities. Consequently, the absolute accuracy, particularly near the stall, may not be high.

4.4. *Pitching Moment.*—The values of C_m about the aerofoil quarter-chord point are plotted against Mach number in Fig. 11 for two values of $C_L = 0\cdot7$, and $1\cdot0$. For lower values of C_L, the changes in C_m will not be so marked and so the curve for $C_L = 0\cdot7$ represents the greatest variation that is likely to be encountered in the cruising range. For this C_L value, there is little change up to $M = 0\cdot55$; with further increase in M, the nose-down moment increases. Even for $C_L = 1\cdot0$, it will be seen that the changes are not serious up to $M = 0\cdot6$. These conclusions could have been deduced from the pressure distributions (Fig. 3, 9). The changes at high Mach number are caused by the increases in suction over the rear half of the section.

It should be noted that the compressibility effects are likely to be less serious for the outboard part of the wing, which is of thinner section. For the wing, as a whole, the variation of C_m with M will probably be less and the effect on the aircraft trim characteristics will depend on the spanwise lift distribution and the tail effectiveness. It does not, however, seem to present any serious problem in the normal operating range.

5. *Discussion of Reynolds Number Effects.*—No scale effect was present for $\alpha = 6$ deg but for higher incidences the C_L *vs.* α curves for differing Reynolds numbers separate. Between 6 and 10 deg, increasing the Reynolds number results in a higher value of $dC_L/d\alpha$ being maintained (Fig. 15) in a manner analogous to that illustrated for low-drag sections in Ref. 3. The comparison of the pressure distributions for $\alpha = 9\cdot75$ deg given in Fig. 12 shows that the increase in lift results from a general increase of suction over most of the upper surface and also of pressure on the lower surface.

Fig. 15 shows that for incidences above 10 deg, the flow apparently becomes unstable and two quite distinct C_L *vs.* α curves can be obtained at all Reynolds numbers—on the first (A), C_L begins to fall but then flattens out; while on the second (B), C_L continues to increase with α. Typical pressure distributions corresponding to the two different values of lift are illustrated in Fig. 16 (for $\alpha = 11\cdot7$ deg, $R = 9\cdot3 \times 10^6$). It will be noted that distribution A which gives the lower lift, has the shape, involving a marked separation at about $0\cdot5c$, which becomes standard with increasing Mach number up to $0\cdot5$. Distribution B, on the other hand, is somewhat similar to what is obtained after shock waves have appeared (Figs. 4a, 9). It is likely that for this type of low drag section distribution B is unstable and any fluctuations in the tunnel flow cause the separation to move rapidly forward to the $0\cdot5c$ position. If the incidence had been increased at constant tunnel speed, the well known hysteresis effect might have produced curve B with less uncertainty—*see* also section 7. It is not thought that the fact that no distribution of shape B was recorded for $\alpha = 14$ deg at the highest Reynolds number has any particular significance. Fig. 15 shows that increasing the Reynolds number from $2\cdot9 \times 10^6$ to $9\cdot45 \times 10^6$ seems to have little effect on the phenomenom. Fig. 13, which compares the distributions of shape A for the three Reynolds numbers for $\alpha = 13\cdot6$ deg is, in fact, very similar to Fig. 12 for $\alpha = 9\cdot75$ deg.

Fig. 14 compares the variation with Reynolds number of:—

    (i) the maximum lift values obtained from the distribution ' A ' (these roughly agree with the C_L values where curves A and B diverge),

    (ii) the highest C_L values obtained with curves B,

    (iii) the $C_{L\,max.}$ values given in Ref. 3, and 6 for the NACA 64, 2—418 section.

The NACA 64, 2—418 section is very similar in shape to the Brabazon section in all particulars except for its maximum thickness which is only 18 per cent instead of 21 per cent. Unfortunately, no data are available, for example, on NACA 64, 2—420 directly to show the effect of thickness but judging from the data on other sections, $e.g.$, the NACA 65 series, given in Ref. 6, increasing thickness will result in a drop in $C_{L\,max}$. It appears that this decrease in $C_{L\,max}$ should be about 0·06 for $R = 6 \times 10^6$ and 0·12 for $R = 9 \times 10^6$. Therefore, the values of $C_{L\,max}$ that would be expected for the Brabazon section on the basis of the American data would be about 1·45 for $R = 6 \times 10^6$ and 1·49 for $R = 9 \times 10^6$. The shape of the $C_{L\,max}$ $vs.$ R curve would agree with that found from the R.A.E. tests but the latter give $C_{L\,max}$ values lower by about 0·23 if the ' A ' values are taken or 0·14 at the most if the more optimistic ' B ' values are accepted. Some possible explanations are discussed in para. 7 but it should be noted that Ref. 6 suggests the quoted $C_{L\,max}$ values from the NACA tests may be 0·05 too high, owing to an unexpected change in the empty tunnel pressure measurements during this particular test series.

Fig. 15 shows that the present tests have not been extended to a sufficiently high incidence to reach $C_{L\,max}$ for the B curves and hence the resultant discrepancy between the Brabazon I results and those predicted from the NACA tests is really quite small, if it is assumed that with a different tunnel technique and extended incidence range, lift curves of the shape B would be obtained.

The present tests were also not extended to high enough incidence to compare the post-stall C_L $vs.$ α curves at different Reynolds numbers with those given in Ref. 3 for NACA 64, 2—418 but since even curves A are not showing any tendency to fall rapidly 4 deg beyond the onset of the stall, it seems likely that the shapes may be similar (except for more fluctuation round the peak value).

6. *Comparison with Calculated Potential Flow Pressure Distributions.*—Fig. 17 compares the pressure distribution obtained for $\alpha = 0$ deg and $M = 0\cdot3$ with that calculated for incompressible flow by Squire using the second approximation in the Goldstein method. Very good agreement has been obtained, particularly as the compressible flow correction appropriate for $M = 0\cdot3$ would account for more than half the discrepancy in the upper surface peak suctions. Good agreement was similarly obtained for $\alpha = 4$ and 6 deg both in the pressure distribution shapes and in the integrated lift values. This agreement can be considered very gratifying.

7. *Application of Tunnel $C_{L\,max}$ Value to Flight Conditions.*—There are three principal doubtful aspects in the deduction from the tunnel tests of the $C_{L\,max}$ values to be expected under flight conditions. These are discussed below :—

(i) *Tunnel Constraint.*—The usual tunnel constraint corrections probably become unreliable at high incidence with large values of aerofoil chord/tunnel height. Since the flow between the aerofoil upper surface and the tunnel wall could be considered as the flow in a divergent channel, it follows that the walls impose an adverse pressure gradient which might induce an earlier separation and a lower $C_{L\,max}$. It is hoped, however, that it is only the C_L $vs.$ α curve and not the absolute values of $C_{L\,max}$ that are affected. (The wall pressures showed that the supersonic region did not extend to the wall even for $M = 0\cdot7$).

(ii) *Hysteresis Effects.*—The tests were made by varying the speed at an aerofoil incidence and not by varying the incidence at a fixed speed. The latter is the more usual and preferable technique since it represents practical conditions, particularly the effect of up-gusts. It is a well known phenomenon that higher $C_{L\,max}$ values are obtained when the incidence is increasing than when it is preset at a high value in the stalling range. R. & M. 1648[7] shows that the

7

difference may amount to 15 or 20 per cent and also, significantly, that the higher C_L vs. α curve may resemble curve 'B' of Fig. 16. It seems likely, therefore, that a curve of shape ' B ' would result from a test made with the more suitable technique and also that the $C_{L\,max.}$ values up to $M = 0.6$ might be at least 1.3. It seems that this important effect should be investigated further.

(iii) *Interaction of Effects of Reynolds Number and Mach Number.*—As was explained earlier, Reynolds number effects on $C_{L\,max.}$ are likely to be less important at high Mach number since the flow will probably be turbulent after the shock wave. Increasing Reynolds number might remove the inflexion in the $M = 0.6$ curve (in view of the effects at low Mach number) and this effect may perhaps be predicted with some confidence since the flight results* of Ref. 4 show $C_{L\,max.}$ vs. M curves similar in shape to those given here, *i.e.*, a rise in $C_{L\,max.}$ at values of M just below that at which $C_{L\,max.}$ begins to fall rapidly.

It will be noted that all the above are reasons why the tunnel $C_{L\,max.}$ values may be pessimistic and, therefore, can be taken as a conservative estimate of what may be expected in flight.

8. *Conclusions.*—The pressure distribution measurements on the Brabazon I wing root section have shown that:—

(i) No serious changes in C_L or C_m occur under the cruising conditions of the aircraft. The form drag is beginning to rise rapidly at $M = 0.6$.

(ii) The value of $C_{L\,max.}$ (taken as the lowest value for which $\partial C_L/\partial \alpha = 0$) remains roughly constant at about 1.15 up to $M = 0.6$, and then falls to 1.01 for $M = 0.7$ (at $R = 3 \times 10^6$).

(iii) For $M = 0.2$, $C_{L\,max.}$ increases from 1.17 for $R = 3 \times 10^6$ to 1.26 for $R = 9.45 \times 10^6$.

(iv) The maintenance of the same $C_{L\,max.}$ values up to $M = 0.6$ despite the 21 per cent thickness ratio, results from the far back peak suction, particularly after the appearance of shock waves.

(v) The increasing lift contribution from the back $0.5c$ has an appreciable influence only for Mach numbers above that at which $C_{L\,max.}$ begins to decrease.

(vi) The two C_L vs. α curves beyond the stall at low Mach number probably indicate that the pressure distribution having no marked separation is unstable and susceptible to tunnel fluctuations which are liable to cause a separation at about $0.5c$.

(vii) The low speed $C_{L\,max.}$ values are lower than would be deduced from NACA tests on similar aerofoils. The difference amounts to about 0.23, using the lowest values deduced from the present tests but is not more than 0.14, if the higher values are taken. Contributory causes of the discrepancy are:—

    (a) The incidence range covered was not high enough.

    (b) A quoted uncertainty of 0.05 in the NACA results.

    (c) Tunnel constraint in the R.A.E. tests.

    (d) Hysteresis effects, the R.A.E. tests being at constant incidence and varying speed (this effect might amount to 15 to 20 per cent).

The margin between cruising and stalling conditions seems adequate to provide manoeuvrability and safety in up-gusts. The tests however suggest several directions in which further research would be very valuable.

---

* Obtained from records of buffeting, etc., a marked inflexion in the lift curve should induce buffeting.

REFERENCES

No.	Author	Title, etc.
1	J. S. Thompson, D. Adamson ..	High-speed Wind-tunnel Measurements of Pressure Distribution on an aerofoil of N.A.C.A. 23021 section. R.A.E. Report No. Aero 1985, A.R.C. 8350. November, 1944. (Unpublished).
2	F. N. Kirk	Effects of Mach Number on Maximum Lift. R.A.E. Technical Note No. Aero 1867. A.R.C. 10463. January, 1947. (Unpublished).
3		Note on the Scale Effect of Low-Drag Wing Sections between Wind Tunnel and Flight Conditions. A.R.C. 10,376. Aero Discussion Note No. 13. January, 1947. (Unpublished).
4	Spreiter, Steffen	Effect of Mach Number and Reynolds Numbers on Maximum Lift Coefficient. N.A.C.A. Technical Note No. 1044. March, 1946.
5	Thompson, Markowicz, Beavan, Fowler.	Pressure Distribution and Wake Traverses on Models of Mustang Wing Section in the R.A.E. and N.P.L. High Speed Tunnels. R. & M. 2251. August, 1944.
6	Jacobs, Abbott, and Davidson ..	Preliminary Low Drag Aerofoil and Flap Data from Tests at Large Reynolds Numbers and Low Turbulence. Reproduced in A.R.C. Report No. 5846. May, 1942. (Unpublished).
7	Farren	Reaction on a Wing whose Incidence is Changing Rapidly. Wind-tunnel Experiments with a Short Period Recording Balance. R. & M. 1648. January, 1935.

TABLE 1

Brabazon I. Wing Root Section

All ordinates are expressed as fractions of the chord.
Leading edge radius $= 0 \cdot 027c$.

Distance from Leading edge	Ordinates of Upper Surface	Ordinates of Lower Surface
0	0	0
0·002	0·011	0·010
0·005	0·018	0·015
0·010	0·026	0·020
0·025	0·043	0·030
0·050	0·061	0·041
0·100	0·087	0·053
0·150	0·105	0·061
0·200	0·119	0·066
0·250	0·128	0·069
0·300	0·135	0·071
0·350	0·138	0·072
0·400	0·138	0·071
0·450	0·133	0·067
0·500	0·124	0·062
0·550	0·114	0·056
0·600	0·101	0·049
0·650	0·088	0·041
0·700	0·074	0·034
0·750	0·060	0·027
0·800	0·046	0·020
0·850	0·032	0·013
0·900	0·019	0·007
0·925	0·014	0·005
0·950	0·008	0·003
0·975	0·004	0·001
1·000	0	0

TABLE 2

Positions of Pressure Plotting Holes on Brabazon I Wing Root Section

All distances are given as fractions of chord.

Upper Surface		Lower Surface	
No. of P.P. Hole	Distance from Leading Edge	No. of P.P. Hole	Distance from Leading Edge
1	0	—	—
2	0·013	29	0·012
3	0·025	28	0·025
4	0·050	27	0·050
5	0·101	26	0·101
6	0·150	25	0·151
7	0·201	24	0·200
8	0·251	23	0·251
9	0·300	22	0·300
10	0·401	21	0·400
11	0·497	20	0·498
12	0·599	19	0·598
13	0·699	18	0·699
14	0·823	17	0·818
15	0·949	16	0·949
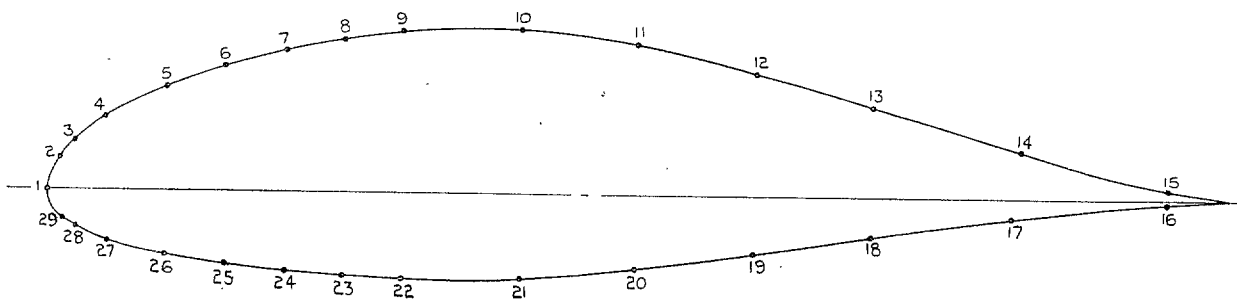
Fig. 1.   Brabazon I wing root section.
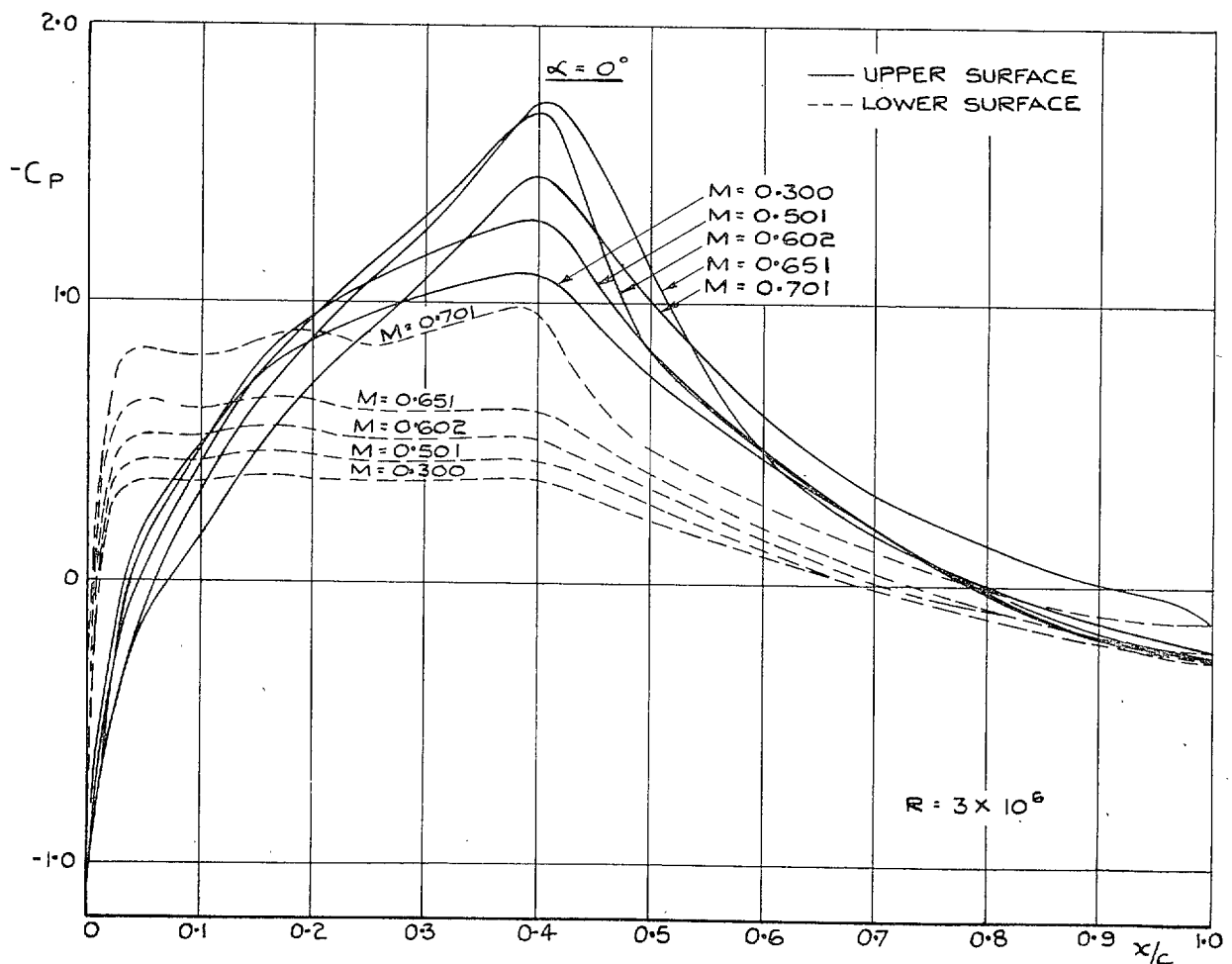
Fig. 2a.   Variation of pressure distribution with Mach number.
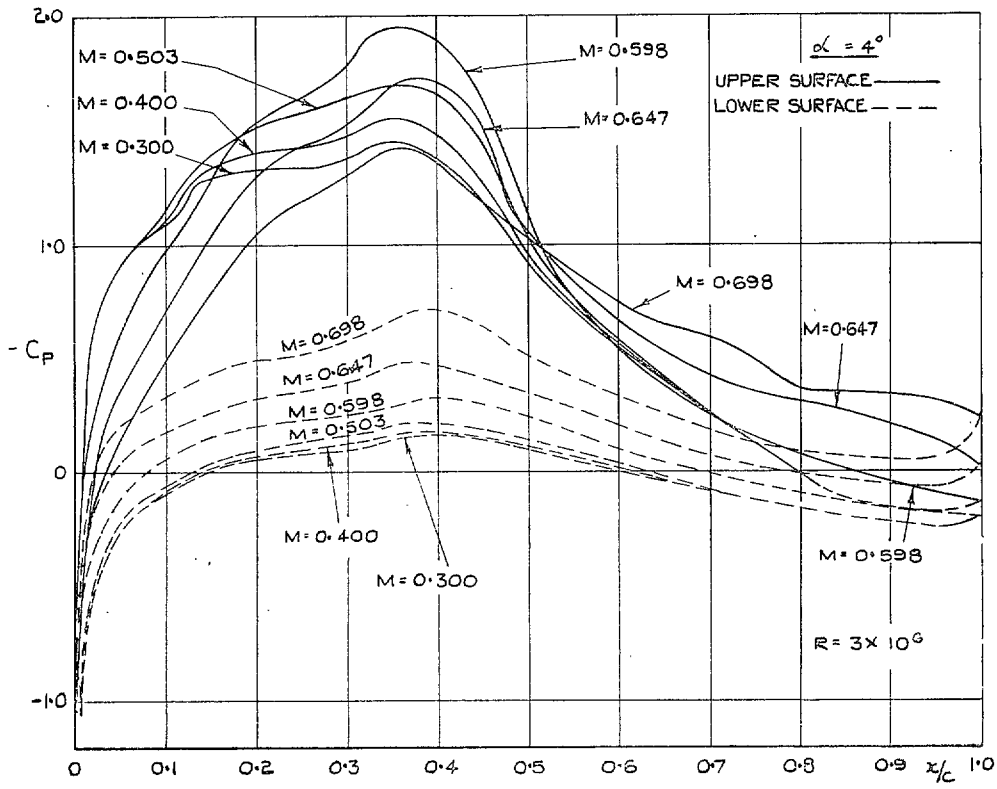
Fig. 2b. Variation of pressure distribution with Mach number.
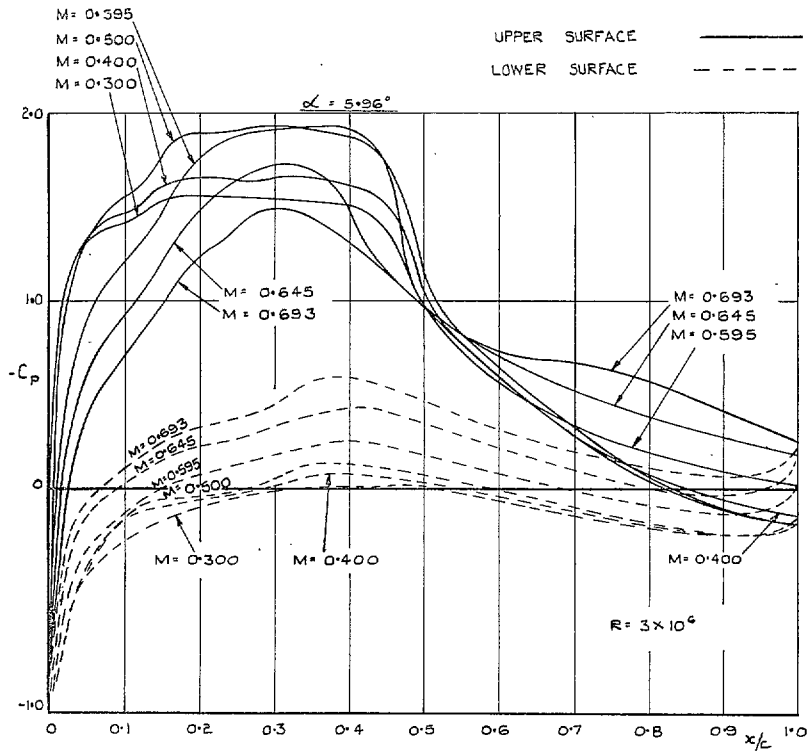
Fig. 2c. Variation of pressure distribution with Mach number.

13
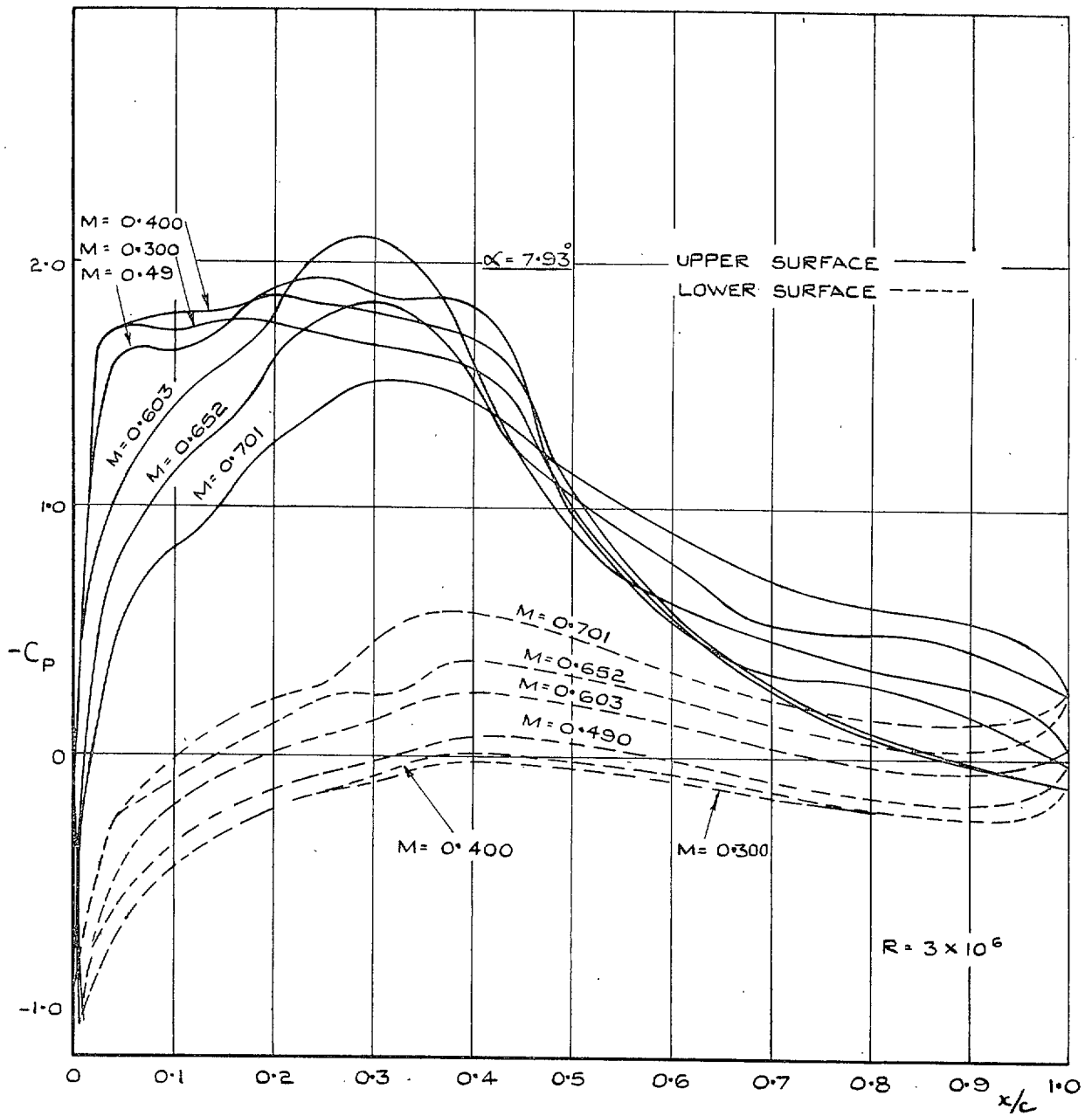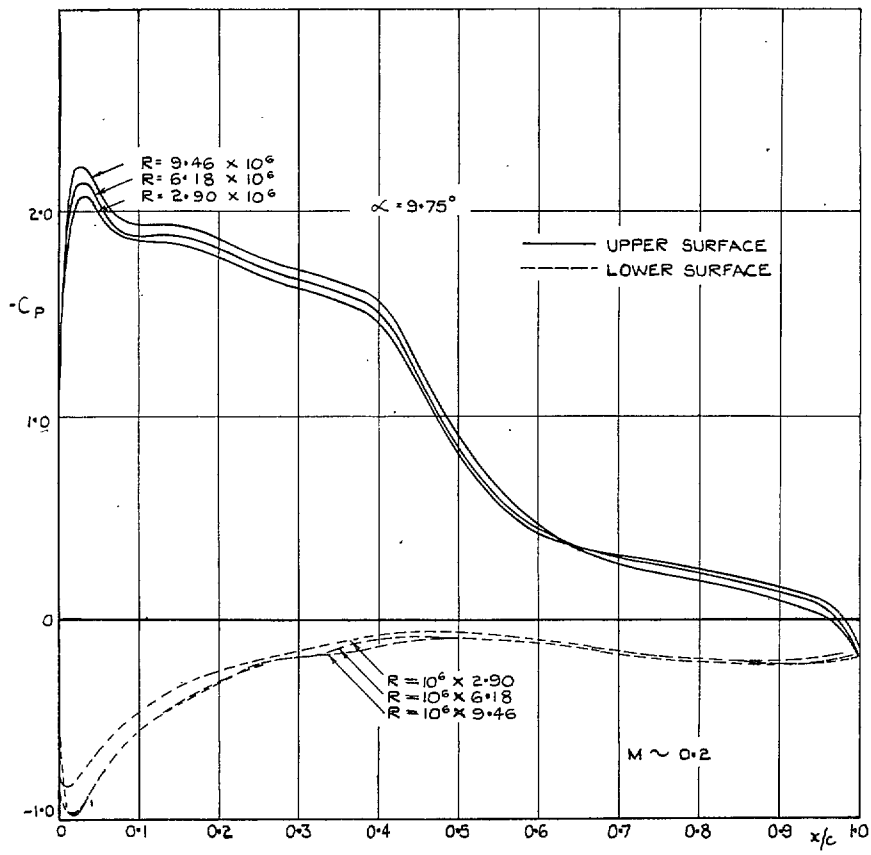
Fig. 2d.　Variation of pressure distribution with Mach number.
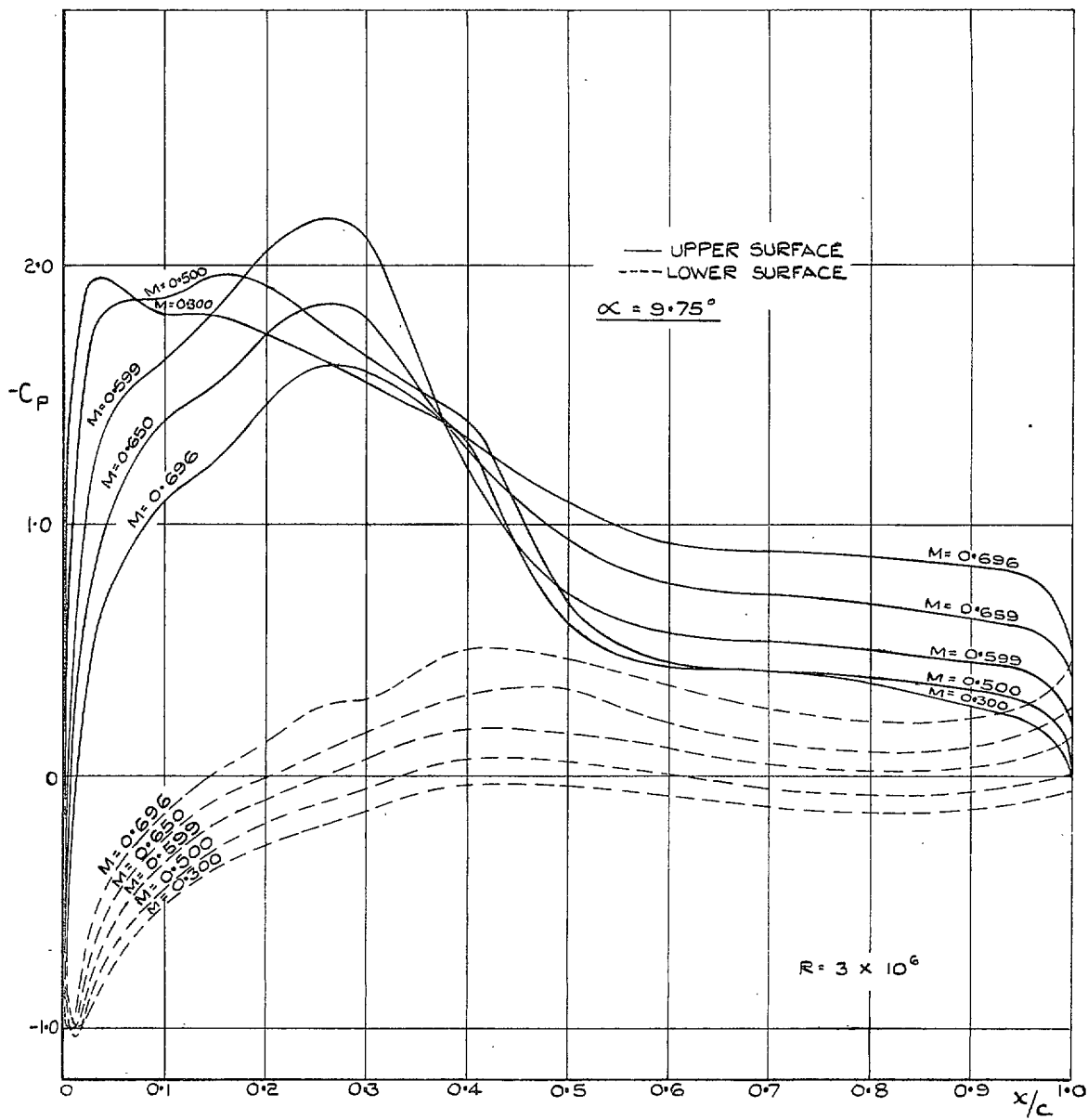
Fig. 3. Variation of pressure distribution with Mach number.
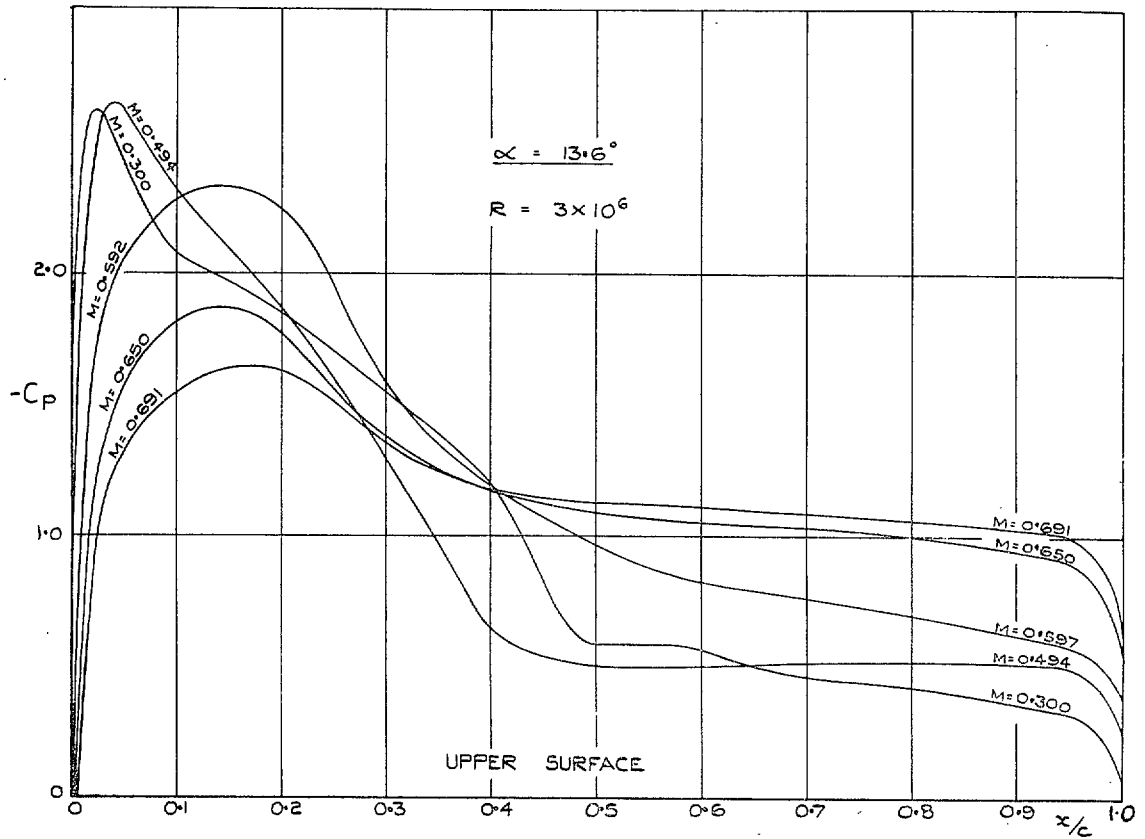
Fig. 4a. Variation of pressure distribution with Mach number.
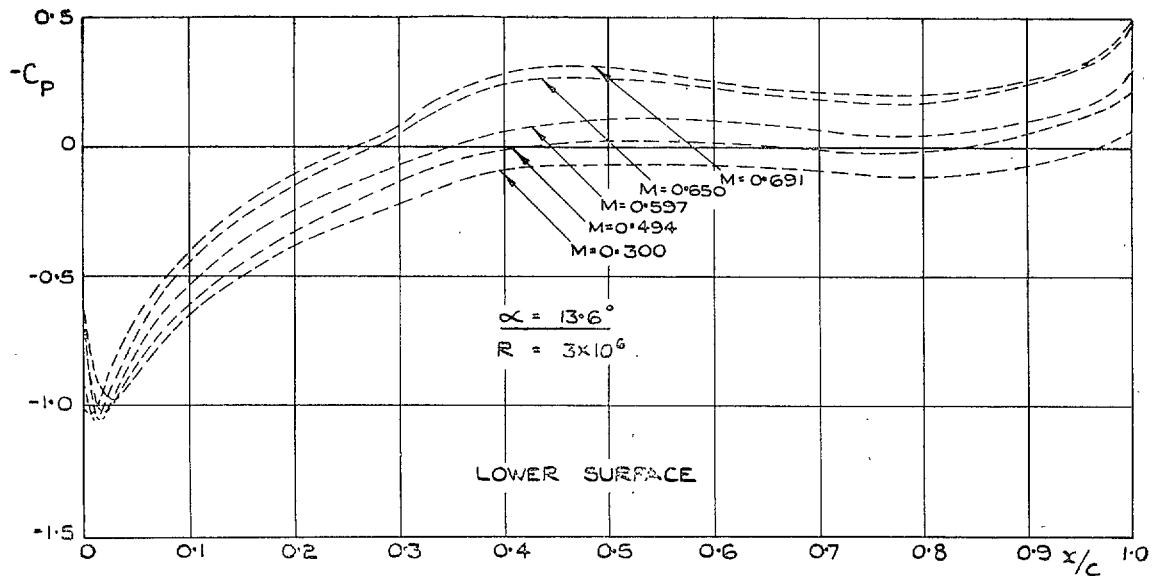
Fig. 4b. Variation of pressure distribution with Mach number.
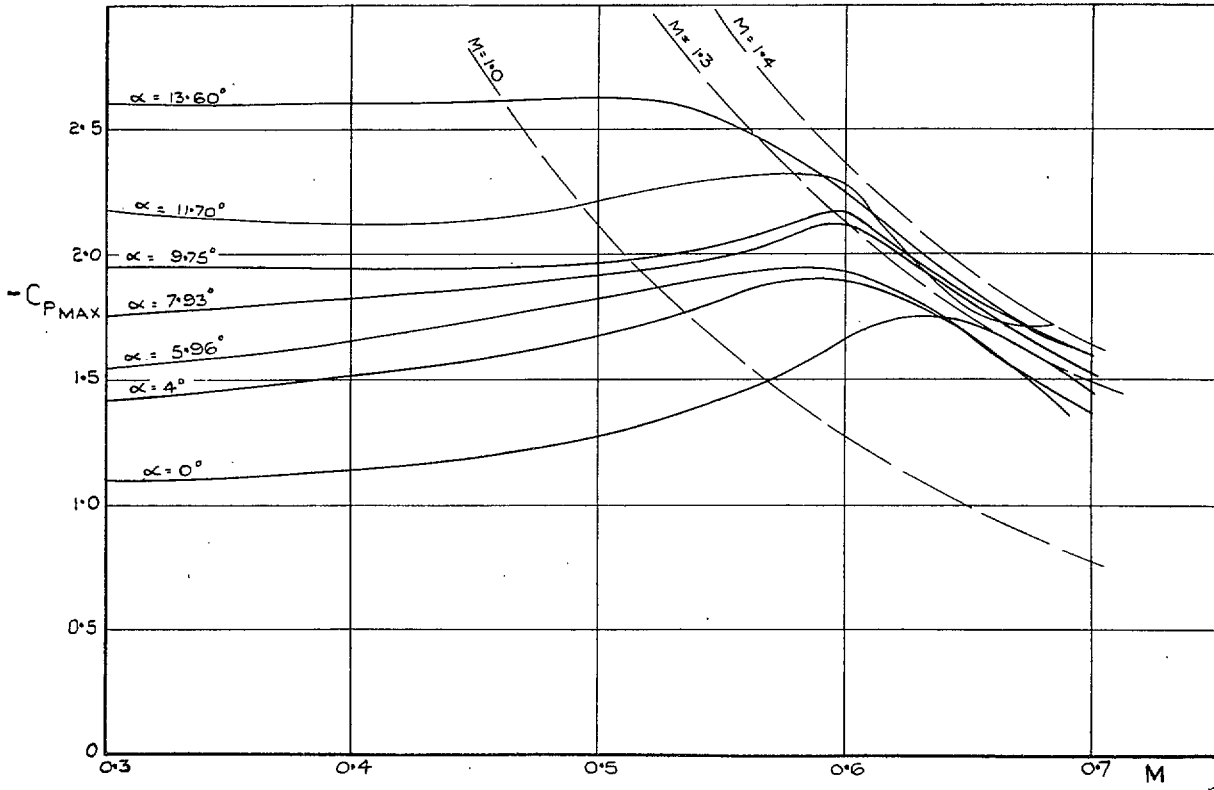
Fig. 5.   Variation of maximum C_p with Mach number.

Fig. 6.   Lift carpet.

17
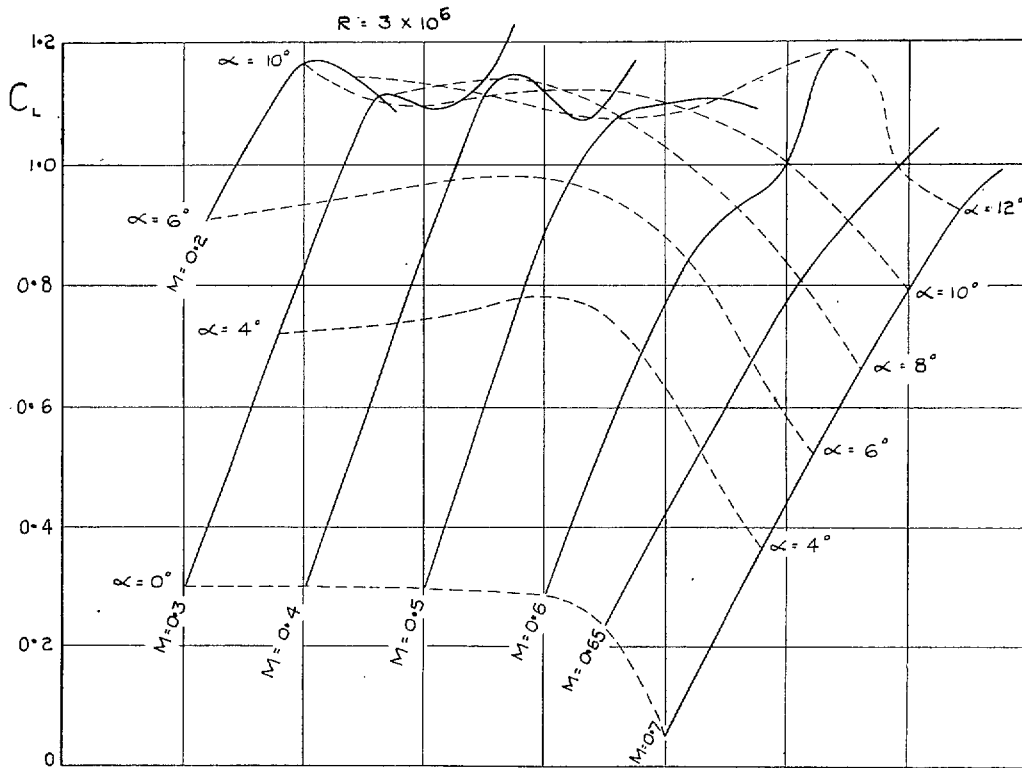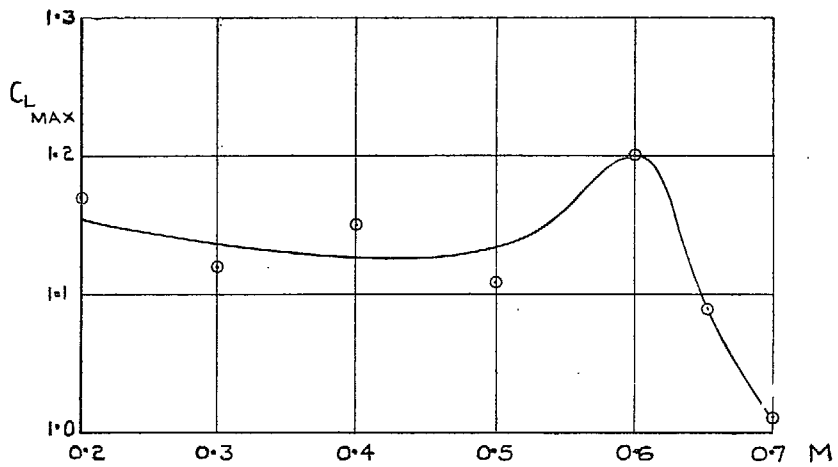
Fig. 7a. Variation of $C_{L\ max.}$ with Mach number.
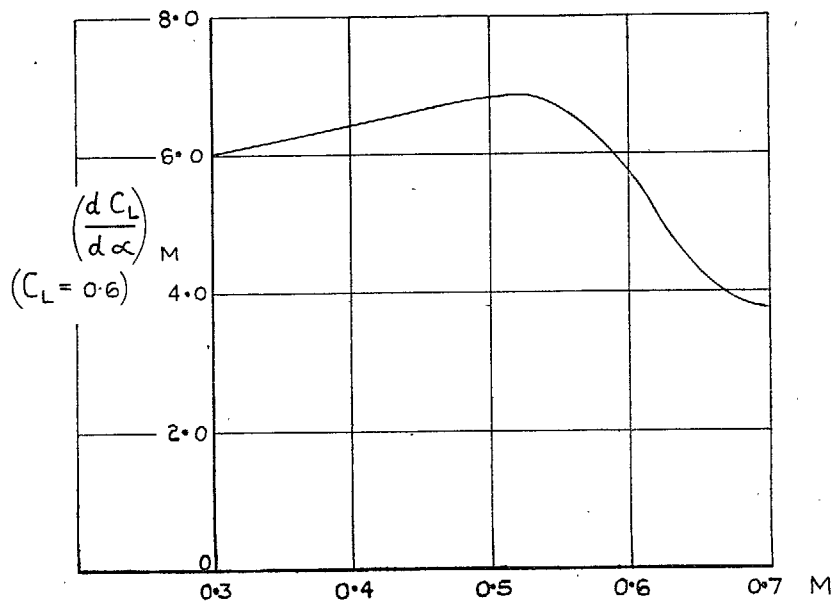
Fig. 7b. Variation of $(dC_L/d\alpha)_M$ with Mach number.

INCIDENCE FROM
ZERO LIFT

----- N A C A 23021 R = 2×10⁶
——— BRABAZON I R = 3×10⁶
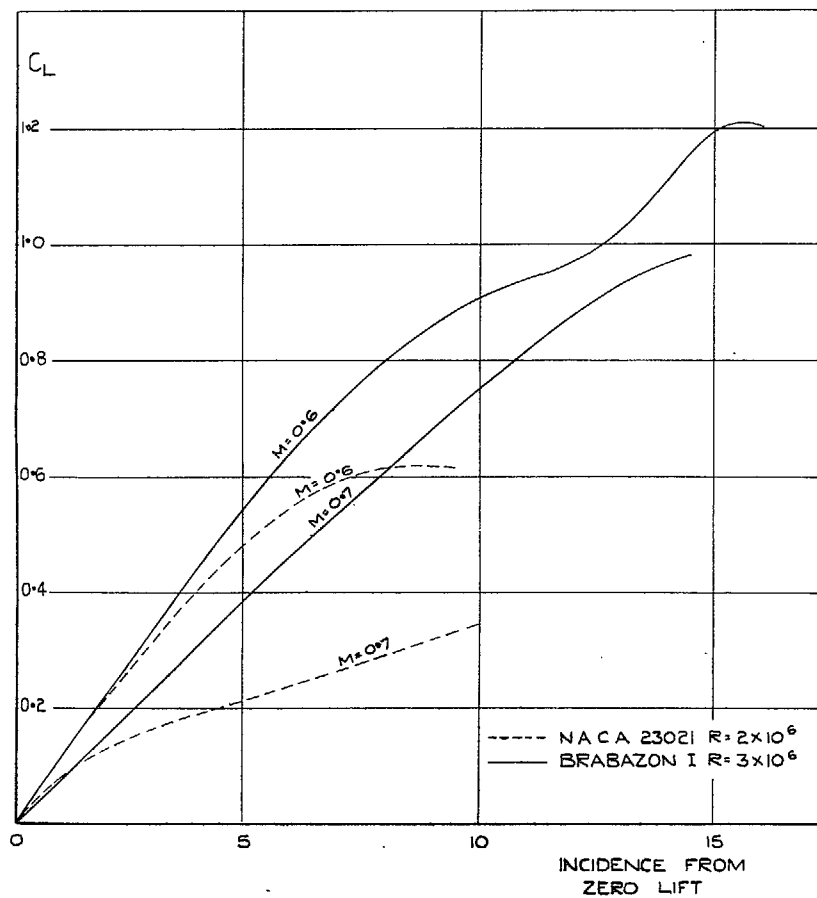
Fig. 8. Comparison of lift curves for NACA 23021 and Brabazon 1 sections.

18
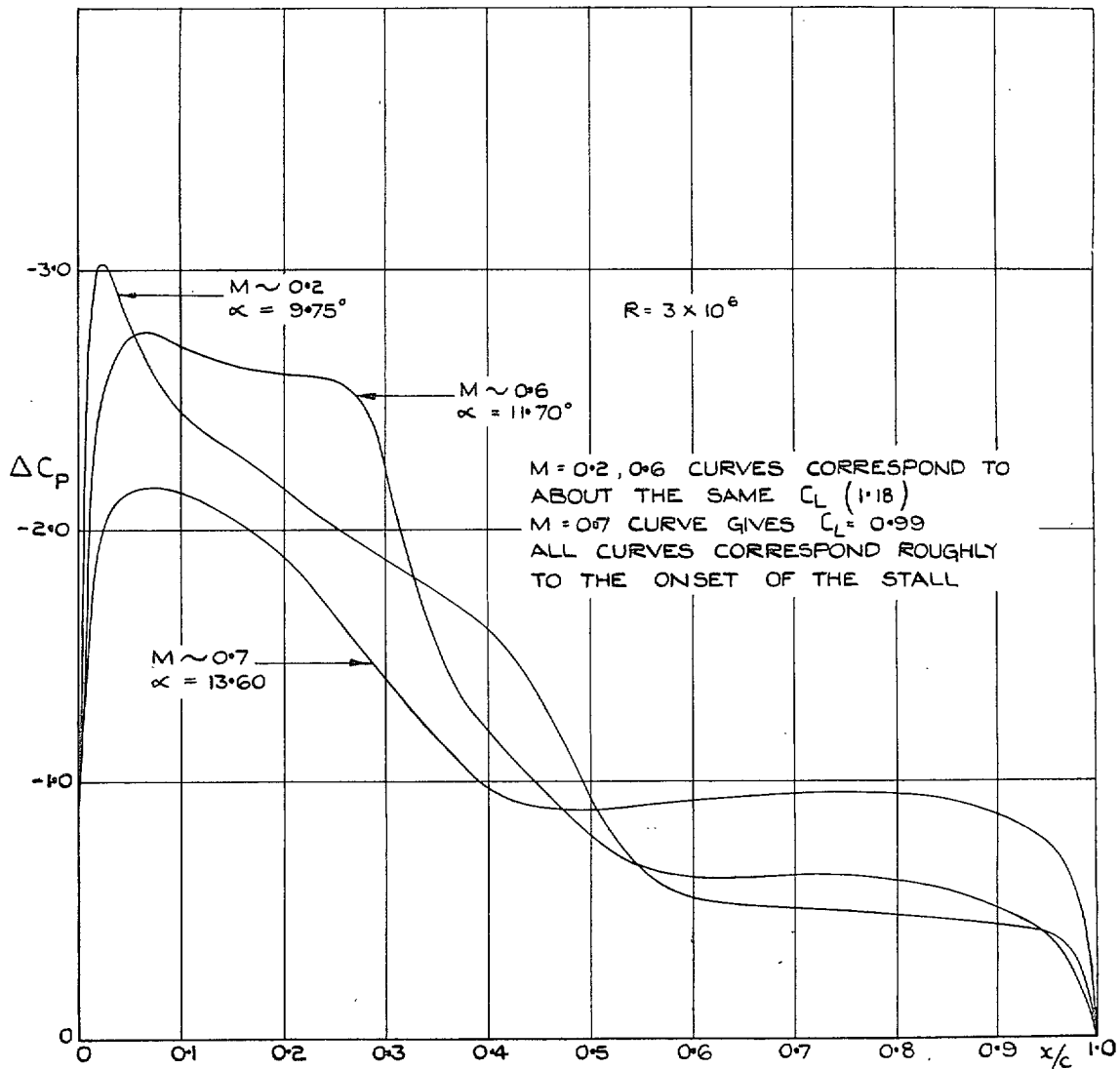
Fig. 9. Comparison of lift loadings along the chord at varying Mach number and incidence.

19
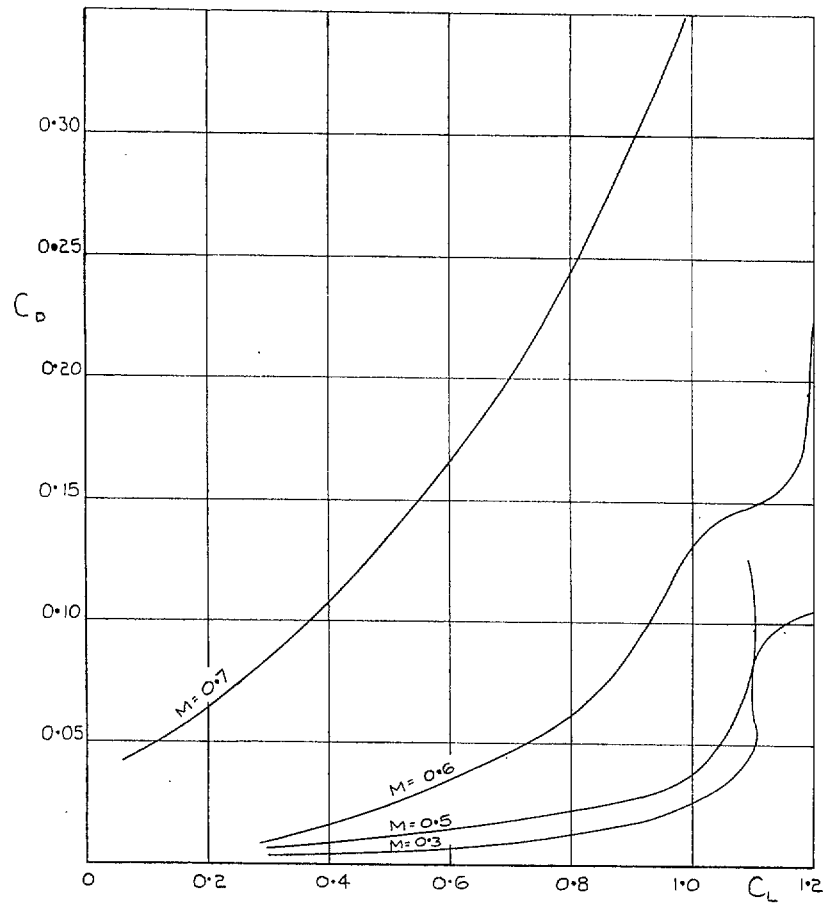
Fig. 10.   Variation of form drag with lift at constant Mach number.
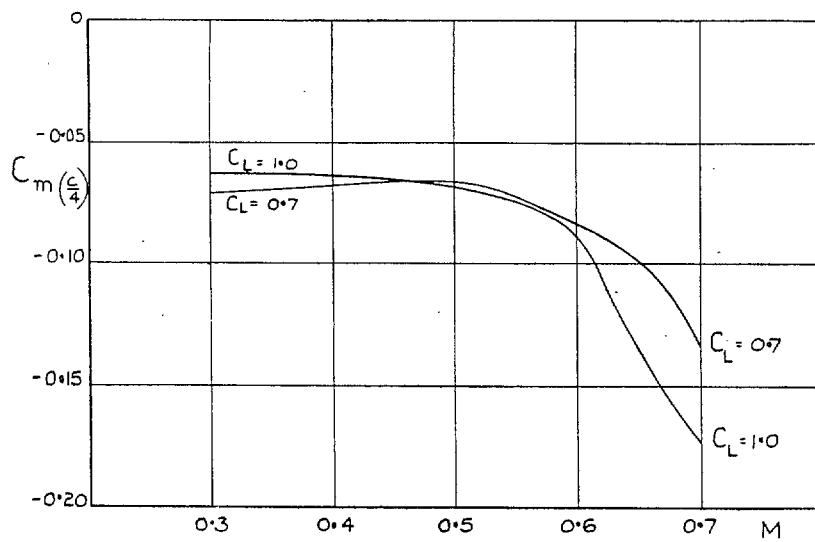
Fig. 11.   Variation of $C_{m\,c/4}$ at constant C_L, with Mach number.

20

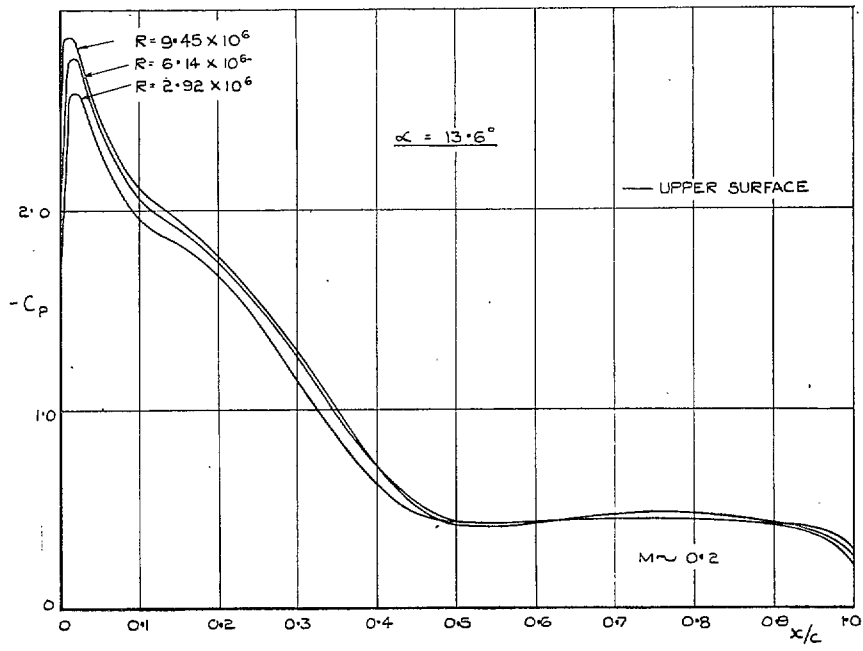Fig. 12. Variation of pressure distribution with Reynolds number.

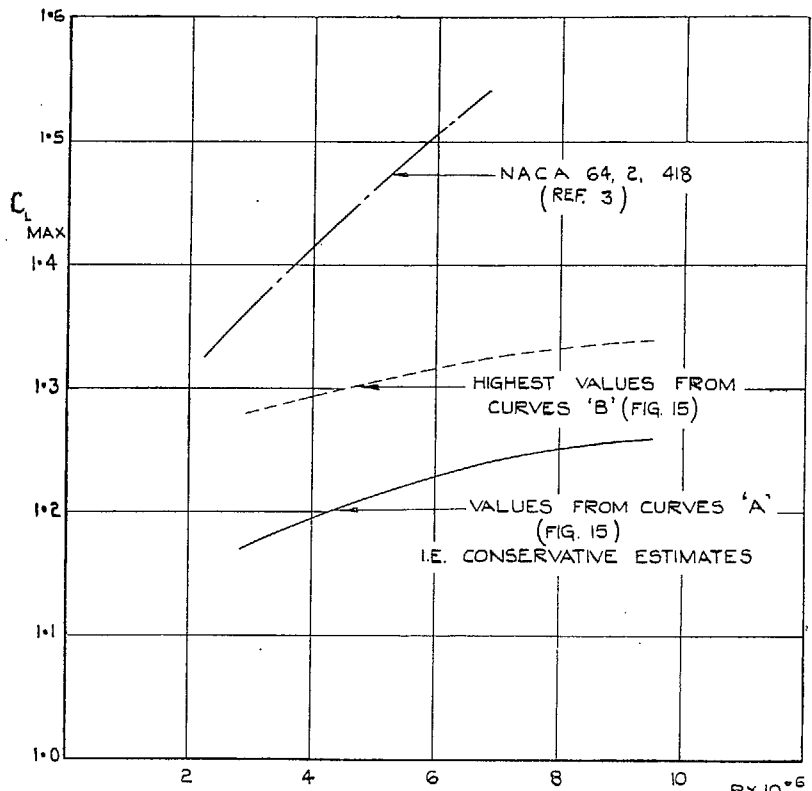Fig. 13. Variation of upper-surface pressure distribution with Reynolds number.

21

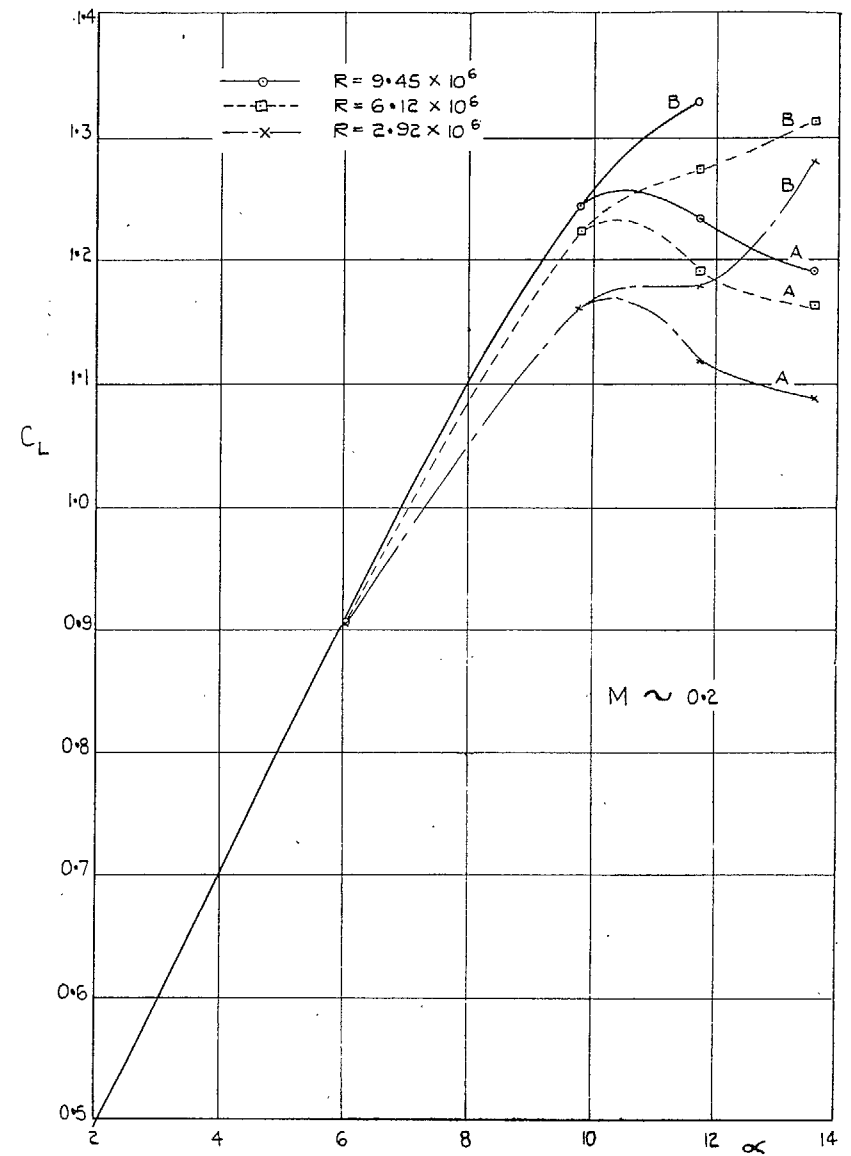Fig. 14. Variation of $C_{L\,max}$ with Reynolds number.

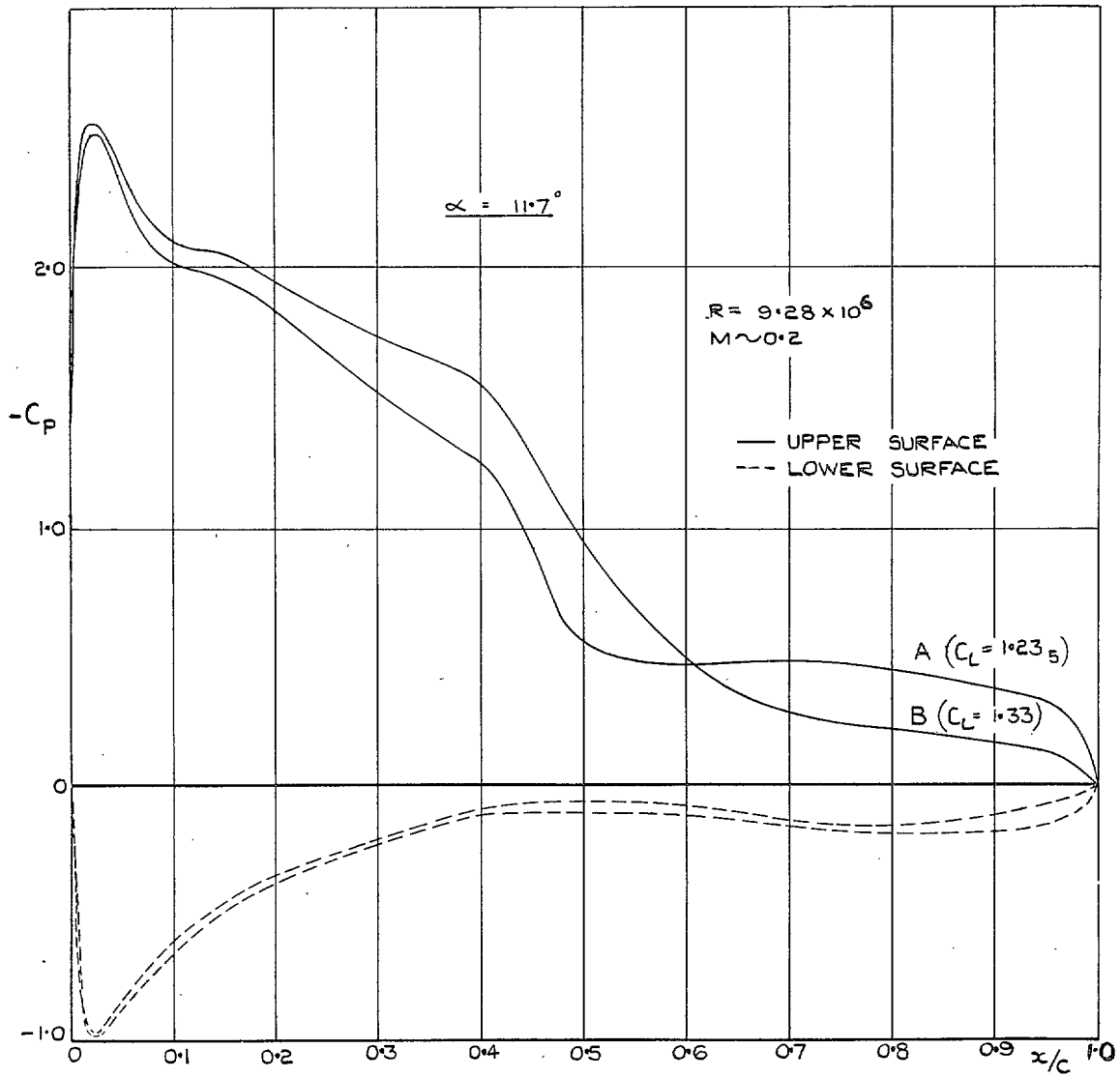Fig. 15. Variation of C_L with incidence at various Reynolds numbers.

Fig. 16. Comparison of the two pressure distribution shapes obtained at high incidence and low Mach number.
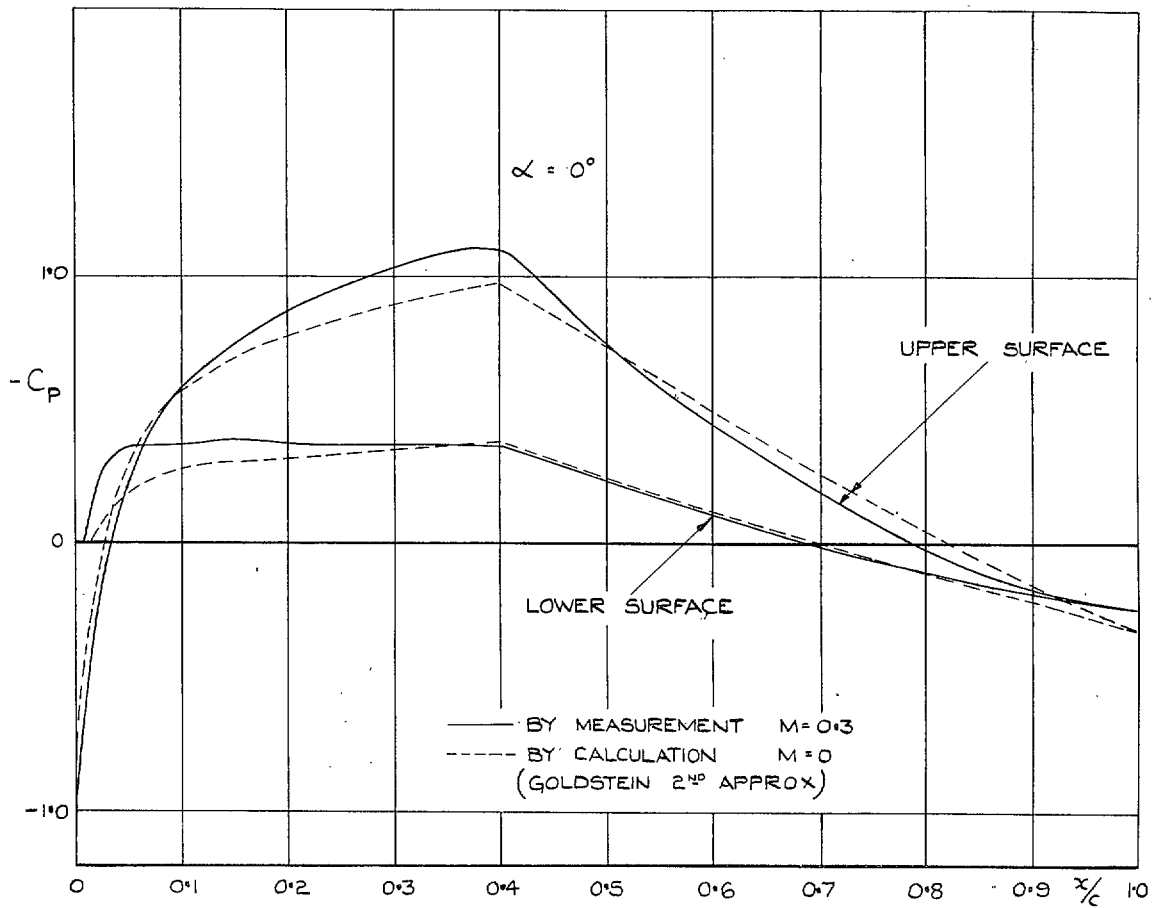
Fig. 17. Comparison of calculated and measured low speed pressure distributions.

Publications of the
Aeronautical Research Council

ANNUAL TECHNICAL REPORTS OF THE AERONAUTICAL RESEARCH COUNCIL (BOUND VOLUMES)—

1934-35 Vol. I. Aerodynamics. *Out of print.*
        Vol. II. Seaplanes, Structures, Engines, Materials, etc. 40s. (40s. 8d.)

1935-36 Vol. I. Aerodynamics. 30s. (30s. 7d.)
        Vol. II. Structures, Flutter, Engines, Seaplanes, etc. 30s. (30s. 7d.)

1936 Vol. I. Aerodynamics General, Performance, Airscrews, Flutter and Spinning. 40s. (40s. 9d.)
        Vol. II. Stability and Control, Structures, Seaplanes, Engines, etc. 50s. (50s. 10d.)

1937 Vol. I. Aerodynamics General, Performance, Airscrews, Flutter and Spinning. 40s. (40s. 10d.)
        Vol. II. Stability and Control, Structures, Seaplanes, Engines, etc. 60s. (61s.)

1938 Vol. I. Aerodynamics General, Performance, Airscrews. 50s. (51s.)
        Vol. II. Stability and Control, Flutter, Structures, Seaplanes, Wind Tunnels, Materials. 30s. (30s. 9d.)

1939 Vol. I. Aerodynamics General, Performance, Airscrews, Engines. 50s. (50s. 11d.)
        Vol. II. Stability and Control, Flutter and Vibration, Instruments, Structures, Seaplanes, etc. 63s. (64s. 2d.)

1940 Aero and Hydrodynamics, Aerofoils, Airscrews, Engines, Flutter, Icing, Stability and Control, Structures, and a miscellaneous section. 50s. (51s.)

Certain other reports proper to the 1940 volume will subsequently be included in a separate volume.

ANNUAL REPORTS OF THE AERONAUTICAL RESEARCH COUNCIL—

1933-34	1s. 6d. (1s. 8d.)
1934-35	1s. 6d. (1s. 8d.)
April 1, 1935 to December 31, 1936.	4s. (4s. 4d.)
1937	2s. (2s. 2d.)
1938	1s. 6d. (1s. 8d.)
1939-48	3s. (3s. 2d.)

INDEX TO ALL REPORTS AND MEMORANDA PUBLISHED IN THE ANNUAL TECHNICAL REPORTS, AND SEPARATELY—

April, 1950   R. & M. No. 2600. 2s. 6d. (2s. 7½d.)

INDEXES TO THE TECHNICAL REPORTS OF THE AERONAUTICAL RESEARCH COUNCIL—

December 1, 1936 — June 30, 1939.	R. & M. No. 1850.	1s. 3d. (1s. 4½d.)
July 1, 1939 — June 30, 1945.	R. & M. No. 1950.	1s. (1s. 1½d.)
July 1, 1945 — June 30, 1946.	R. & M. No. 2050.	1s. (1s. 1½d.)
July 1, 1946 — December 31, 1946.	R. & M. No. 2150.	1s. 3d. (1s. 4½d.)
January 1, 1947 — June 30, 1947.	R. & M. No. 2250.	1s. 3d. (1s. 4½d.)

Prices in brackets include postage.

Obtainable from

HER MAJESTY'S STATIONERY OFFICE

York House, Kingsway, LONDON, W.C.2   429 Oxford Street, LONDON, W.1
P.O. Box 569, LONDON, S.E.1
13a Castle Street, EDINBURGH, 2   1 St. Andrew's Crescent, CARDIFF
39 King Street, MANCHESTER, 2   Tower Lane, BRISTOL, 1
2 Edmund Street, BIRMINGHAM, 3   80 Chichester Street, BELFAST

or through any bookseller.